tvst

Article

Intraocular Distribution and Kinetics of Intravitreally Injected Antibodies and Nanoparticles in Rabbit Eyes

Hyeong Min Kim[1,*], Seungmin Ha[2,*], Hye Kyoung Hong[1,*], Yoonha Hwang[3,4], Pilhan Kim[3,4,5], Eunsol Yang[6], Jae Yong Chung[6], Sunyoung Park[7], Young Joo Park[1], Kyu Hyung Park[1], Hyuncheol Kim[7], and Se Joon Woo[1]

[1] Department of Ophthalmology, Seoul National University College of Medicine, Seoul National University Bundang Hospital, Seongnam, Republic of Korea
[2] Seoul Eye Clinic, Daegu, Republic of Korea
[3] Graduate School of Nanoscience and Technology, Korea Advanced Institute of Science and Technology (KAIST), Daejeon, Republic of Korea
[4] KI for Health Science and Technology (KIHST), Korea Advanced Institute of Science and Technology (KAIST), Daejeon, Republic of Korea
[5] Graduate School of Medical Science and Engineering, Korea Advanced Institute of Science and Technology (KAIST), Daejeon, Republic of Korea
[6] Department of Clinical Pharmacology and Therapeutics, Seoul National University College of Medicine and Bundang Hospital, Seongnam, Republic of Korea
[7] Department of Chemical and Biomolecular Engineering, Sogang University, Seoul, Republic of Korea

Correspondence: Se Joon Woo, MD, PhD, Department of Ophthalmology, Seoul National University Bundang Hospital, 173-82 Gumi-ro, Bundang-gu, Seongnam-si, Gyeonggi-do, 13620, South Korea.
e-mail: sejoon1@snu.ac.kr

Received: February 4, 2020
Accepted: March 31, 2020
Published: May 20, 2020

Keywords: distribution; intraocular; intravitreal; kinetics; nanoparticles

Citation: Kim HM, Ha S, Hong HK, Hwang Y, Kim P, Yang E, Chung JY, Park S, Park YJ, Park KH, Kim H, Woo SJ. Intraocular distribution and kinetics of intravitreally injected antibodies and nanoparticles in rabbit eyes. Trans Vis Sci Tech. 2020;9(6):20, https://doi.org/10.1167/tvst.9.6.20

Purpose: To investigate the intraocular distribution and kinetics of antibodies and nanoparticles in the experimental model.

Methods: Antibodies (whole IgG 149kDa, antigen-binding fragments 48.39 kDa) and four kinds of nondegradable nanoparticles (25, 50, 200, and 250 nm) were intravitreally injected in the right eye of New Zealand white rabbits. The average optical density and concentration were used to measure intraocular distribution and kinetics.

Results: After intravitreal injection, antibodies were distributed throughout the vitreous humor and eliminated gradually into anterior and posterior routes. Fluorescence intensity decreased 1 day after injection and was not detected 25 days after injection. The nondegradable nanoparticles migrated posteriorly to the retina 7 days after injection onward and anteriorly to the aqueous humor from 1 hour to 1 day after injection. The fluorescence intensity of the nanoparticles was relatively stable in the vitreous humor, compared to antibodies. Nanoparticles accumulated on the internal limiting membrane of the retina with no penetration into deeper retinal tissue, whereas the smaller size 25 nm nanoparticles passed across the ciliary body and moved into choroid, retina, and suprachoroidal space. A gradual decrease of nanoparticles by their sizes in the vitreous after 30 days after injection was described as the percentage ratio: 61.1% (25 nm), 69.1% (50 nm), 78.6% (200nm), and 85.3% (250 nm).

Conclusions: Our study revealed the in vivo intraocular distribution and kinetics of antibodies and nanoparticles with diverse sizes and the result might help to develop newer intraocular drugs and drug delivery systems to treat retinal diseases.

Translational Relevance: These experimental results can be valuable data for human research.

Introduction

In developed countries, age-related macular degeneration is recognized as the leading cause of visual deterioration in patients older than 50 years.[1] Exudative age-related macular degeneration, a subtype of age-related macular degeneration, is caused by the neovascularization of the macular area; thus anti-vascular endothelial growth factor (anti-VEGF) therapies, such as ranibizumab (Lucentis; Genentech, Inc., San Francisco, CA), bevacizumab (Avastin; Genentech, Inc.), and aflibercept (EYLEA; Regeneron, Inc., Tarrytown, NY; and Bayer Healthcare Pharmaceuticals, Berlin, Germany), are the most common treatments.[2] Moreover, anti-VEGF drugs have been used to treat diabetic macular edema and macular edema accompanied by retinal vein occlusion.[3–5] The anti-VEGF drugs, bevacizumab, and ranibizumab are produced as humanized monoclonal antibodies, whole IgG (149 kDa), and antigen-binding fragments (Fab) (48.39 kDa), respectively.[6] Previous studies have investigated the intraocular pharmacokinetics (PK) and intravitreal PK properties of administered antibodies in the rabbit model.[7–9] Our prior study analyzed molecules ranging from 60 Da to 150 kDa in size and developed prediction models of intraocular PK, which propose that molecular properties (primarily molecular weight) are significant in intravitreal PKs.[10] Another study by Hutton-Smith et al.[11] proposed a three-compartment model (aqueous humor, vitreous, and retina) that uses the permeability ratio of the inner limiting membrane (ILM) and retinal pigment epithelium to estimate the molecular concentrations in each compartment.

As discussed elsewhere in this article, numerous investigations regarding intraocular PKs have managed to deal with the biologic antibodies, because the anti-VEGF agents are widely accepted standard treatment options for neovascular retinal diseases.[12,13] However, the anti-VEGF protein drugs have relatively short intraocular half-lives and, thus, frequent intraocular injections are needed for long-term treatment. Nanoparticles could be a suitable drug delivery system because the intraocular retention time could increase, a variety of drugs or genes could be delivered, and the size and the composition of materials could be controlled. Inokuchi et al.[14] proposed that the fluorescein isothiocyanate (FITC)-conjugated liposomes under 600 nm could be an effective method for intraocular drug delivery to the retinal layer; however, this study was limited to topical administration. Another study by Amrite et al.[15] demonstrated that, in periocular administration, the size of the nanoparticles influenced the efficiency of meeting sufficient doses of the retinal drug. However, only a few studies have focused on the nanoparticles, and their intraocular distribution and kinetics. Sakurai et al.[16] reported that the clearance parameters in the vitreous humor were correlated to the particle diameter when injecting three sizes of nanoparticles (50 nm, 200 nm, and 2 μm) intravitreally in rabbit eyes.

In our study, we investigated the intraocular distribution and kinetics of biologic antibodies (whole IgG and Fab fragments) and four different sizes of nondegradable nanoparticles (25, 50, 200, and 250 nm). Fluorescence microscopic imaging of dissected eyeballs was serially performed at different time points after intravitreal injection, and specific optical densities and concentrations of nanoparticles in the three compartments (aqueous humor, vitreous, and retina) were evaluated because the results of intraocular PKs of anti-VEGF antibodies have been studied extensively.[7,9,11–13,17–21] By examining the delivery and clearance mechanism of antibodies and nanoparticles, this study provides a foundation for the further development of nanocarriers for drug administration.

Methods

Preparation of Molecules

Antibodies with large molecular weights, whole IgG and Fab fragments, were used as substitutes for anti-VEGF intraocular drugs such as bevacizumab and ranibizumab. FITC was conjugated as ChromPure human whole IgG and Fab fragments (JacksonImmuno Research, West Grove, PA) with an excitation wavelength of 492 nm and an emission wavelength of 520 nm.

Four different-sized nanoparticles were used in this study, including the micromer- red F (25 nm) and green F (250 nm) (fluorescent nonbiodegradable polystyrene nanoparticle, micromod Partikeltechnologie GmbH, Rostock, Germany), and the Fluoresbrite yellow-green microspheres (Polysciences, Inc., Warrington, PA) (50 nm and 200 nm). The micromer-red F has an excitation wavelength of 552 nm and an emission wavelength of 580 nm, and the solution was prepared as a 10 mg/mL (1.2×10^{14} particles/mg) aqueous suspension with a concentration of 1.2×10^{15} particles/mL. The micromer-green F has an excitation wavelength of 475 nm and an emission wavelength of 510 nm, and the solution was prepared as a 25 mg/mL (1.2×10^{11} particles/mg) aqueous suspension with a concentration of 3.0×10^{12} particles/mL. The Fluoresbrite yellow-green

Table 1. Characteristics of the Various Molecules for the Experimental Model

Molecules	Size	Excitation Wavelength	Emission Wavelength	Solution Concentration
Antibodies (FITC-conjugated)				
Whole IgG	149 kDa	492 nm	520 nm	
Fab fragments	48.39 kDa			
Nanoparticles				
Micromer-red F	25 nm	552 nm	580 nm	1.2×10^{15} particles/mL
Micromer-green F	250 nm	475 nm	510 nm	3.0×10^{12} particles/mL
Fluoresbrite YG microspheres	50 nm	490 nm	525 nm	3.64×10^{14} particles/mL
Fluoresbrite YG microspheres	200 nm			5.68×10^{14} particles/mL

YG, yellow-green.

microspheres have an excitation wavelength of 490 nm and an emission wavelength of 525 nm, which is similar to FITC. The 50 nm solution was a 2.5% aqueous suspension with a concentration of 3.64×10^{14} particles/mL, and the 200 nm solution had a concentration of 5.68×10^{14} particles/mL. We prepared a 10-fold diluted solution of 50 nm and a 100-fold diluted solution of 200 nm for intravitreal injection for the prevention of nanoparticle aggregation in the vitreous, based on performing the serial dilutions of 1/2, 1/5, 1/10, 1/20, 1/50, 1/100, 1/200, 1/500, 1/1000, 1/2000, 1/5000, and 1/10000 of the original aqueous suspension. All four nanoparticles are negatively charged and spherically shaped with plain, no surface decorations. The characteristics of the various molecules included in this study are summarized in Table 1.

Procedures of the Animal Experiment

Approval was obtained from the Seoul National University Bundang Hospital Institutional Animal Care and Use Committee, and the animal experiments were conducted adhering to the guidelines from the Association for Research in Vision and Ophthalmology for animal use in research. All the experimental procedures were similar to our previous PK studies using animal models.[17,18,20–22] In brief, we anesthetized rabbits with 15 mg/kg tiletamine hydrochloride/zolazepam hydrochloride (Zoletil, Virbac laboratories, Carros Cedex, France) and 5 mg/kg of xylazine hydrochloride (Rompun, Bayer Healthcare, Seoul, Korea). Rabbit eyes were dilated with 0.5% tropicamide and 0.5% phenylephrine hydrochloride eyedrops (Mydrin-P, Santen Pharmaceutical Co., Osaka, Japan), and topical anesthesia was applied with 1% proparacaine hydrochloride eyedrops (Alcaine, Alcon Laboratories, Inc., Fort Worth, TX). Disinfection was performed with 10% povidone-iodine solution on the periocular area and 5% povidone-iodine eyedrops on the conjunctiva. All experimental procedures were conducted aseptically.

A total of 104 right eyes from 104 healthy New Zealand white rabbits weighing 1.5 to 2.0 kg and age of 8 to 10 weeks were used for the study; 20 eyes each for the whole IgG and Fab fragments, 24 eyes for the mixture of 25 nm and 250 nm micromer nanoparticles, and 20 eyes each for the 50 nm and 200 nm Fluoresbrite yellow-green microsphere nanoparticles.

Using a 30-gauge needle, all intravitreal injections were performed 1 to 2 mm behind the superotemporal quadrant of the limbus. Solutions of 0.02 ml FITC-conjugated whole IgG (2.0 mg/mL) and 0.02 mL Fab fragments (2.0 mg/mL), 0.03 mL mixed solution of 25 nm (4.08×10^{13} particles) and 250 nm nanoparticles (1.02×10^{11} particles), 0.05 mL 50 nm (1.82×10^{13} particles), and 0.05 mL 200 nm nanoparticles (2.84×10^{11} particles) were injected intravitreally. There was no evidence of ocular inflammation, infection, or other adverse events related to the intravitreal injection.

After the intravitreal injection, right eyes were enucleated at each time point as follows: antibodies (IgG and Fab fragments) at 1 hour, 1 day, 3 days, 10 days, and 25 days; 25 nm and 250 nm micromer nanoparticles at 1 hour, 1 day, 7 days, 14 days, 21 days, and 30 days; and 50 nm and 200 nm Fluoresbrite nanoparticles at 1 hour, 1 day, 7 days, 14 days, and 30 days. In each time point, 4 right eyes per solution group were sacrificed, enucleated, and frozen at –80°C liquefied nitrogen.

Analysis of the Fluorescence Microscopic Imaging and Measurement

A cryotome was used for preparing the horizontal cross-section of a frozen eyeball that would be fit for

the imaging process. Fluorescence microscopic imaging of enucleated frozen eye samples was performed using a laser scanning confocal system modified for wide-field imaging.[23,24] Continuous wave laser modules with output wavelengths at 488 nm and 561 nm were used as excitation sources for 25 nm red F and 250 nm green F nanoparticles. Fluorescence emission signals were detected by multi-alkali photocathode photomultiplier tubes (R9110, Hamamatsu, Japan). Green and red fluorescence signals were detected through emission filters with a bandpass at 500 to 550 nm (FF02-525/50, Semrock, Rochester, NY) and 581.5 to 618.5 nm (FF01-600/37, Semrock). Collinearly aligned excitation laser beams were raster-scanned by a rotating polygonal mirror (MC-5, Lincoln Laser, Phoenix, AZ), and a galvanometer-based scanning mirror (6230H, Cambridge Technology, Watertown, MA) and then delivered to the sample via relay optics. The cross-sectional images were developed by multiple wide-field images, and RGB converted color maps of 25 nm (red fluorescent) and 250 nm (green fluorescent) nanoparticles were obtained by the MATLAB image tool.

The frozen aqueous humor, vitreous, and retina were separated from the eyes, and each sample was analyzed for optical density assay. The frozen samples were defrosted and homogenized by an ultrasonicator for 30 seconds at 4°C. The frozen retinas were lysed by CelLytic MT (mammalian tissue) lysis/extraction reagent (10 mL/g of tissue) (Sigma, Saint Louis, MO).[17,18] The optical density of the four nanoparticles was measured with each specific excitation and emission wavelengths as summarized in Table 1. The standard curves were calculated using the dilutions of the original aqueous suspension, and we derived the concentration (number of particles per milliliter) data from the optical density, number of particles per milligram, and standard curve.

The concentrations of nanoparticles in the vitreous humor were estimated by one-compartment model. The PK analyses were performed, and the parameters of half-life (in days), apparent clearance (in milliliters per day), and apparent volume of distribution (in milliliters) were calculated and documented in Table 2.

Results

Fluorescence Microscopic Imaging

Intraocular distribution microscopic images of the antibodies (whole IgG and Fab fragments) are shown in Figures 1A and 1B, developed by fluorescence (top) and MATLAB (bottom). One hour after intravitreal injection, the antibodies were distributed around the injection site. After 1 day, the antibodies were dispersed into the intraocular space that is a vitreous cavity and the anterior chamber. A gradual decrease of fluorescence intensity was observed starting from day 1. The fluorescent gradient was observed in the posterior vitreous above the retina, anterior vitreous beside the ciliary body, and anterior chamber (Fig. 1C). The gradient indicated the directional movement of molecules outward from the center of vitreous cavity. There was no fluorescent gradient at the posterior of the lens indicating no passage. On day 25, there was no detectable fluorescence of both the IgG and Fab fragments, which suggested the clearance and elimination of the injected antibodies.

The intraocular distribution of the 25 nm and 250 nm micromer nanoparticles from 1 hour to 30 days is shown in Figure 2. According to Figure 2, after intravitreal injection, the nanoparticles shifted anteriorly inside the vitreous from 1 hour to 1 day, and the fluorescence intensity increased in the aqueous humor until day 1 for 25 nm nanoparticles, and day 7 for 250 nm nanoparticles, and then decreased afterward. Moreover, nanoparticles advanced posteriorly toward the retina from 7 days onward after intravitreal injection and accumulated on the retinal layer, specifically the ILM, even on day 30. In Figures 3A and 3B, at 14 days after injection, the red and green fluorescent nanoparticles were observed on the inner retinal surface; however, there seems to be no definite penetration into the deeper level of the retinal structures. Then, Figures 3C to 3H, on 21 days after injection, the 25 nm (red F) nanoparticles passed across the ciliary body and distributed into the uveal tissue reaching posterior choroid, retina, and suprachoroidal

Table 2. Estimated PK Parameters in the Vitreous Humor

Nanoparticles	Size	$t_{1/2}$ (days)	CL (mL/d)	V_d (mL)
Micromer-red F	25 nm	50.94	0.01	1.09
Micromer-green F	250 nm	78.13	0.01	1.32
Fluoresbrite YG microspheres	50 nm	48.78	0.02	1.43
Fluoresbrite YG microspheres	200 nm	66.65	0.02	1.83

CL, apparent clearance; $t_{1/2}$, half-life; V_d, apparent volume of distribution; YG, yellow-green.

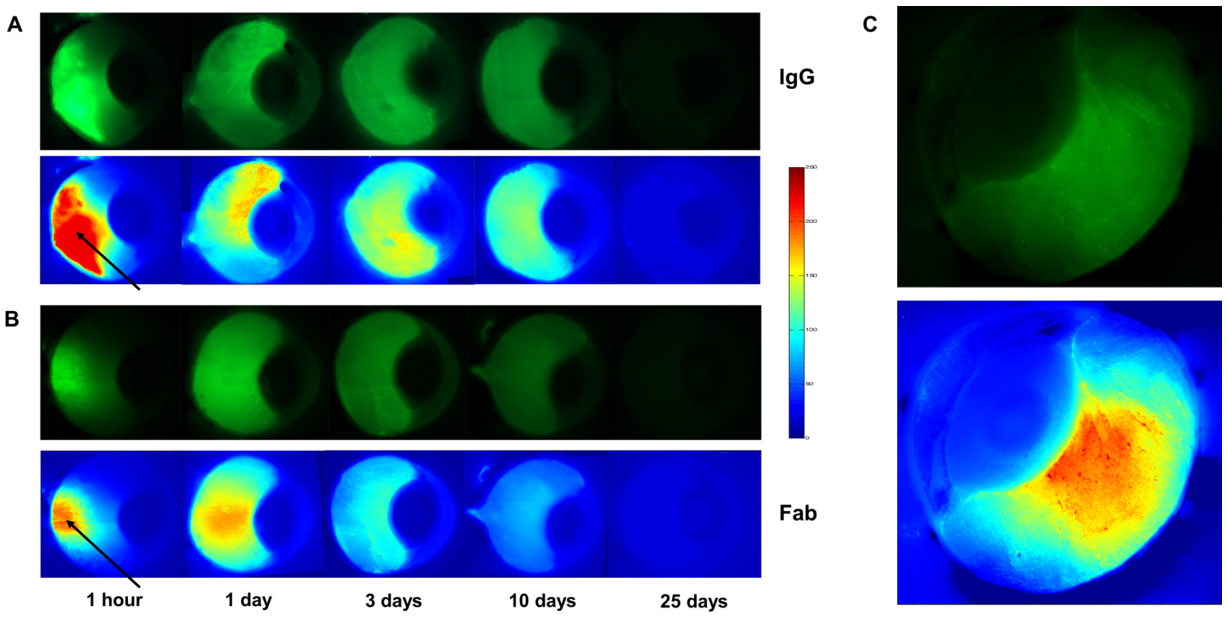

Figure 1. Serial images of the intraocular distribution of FITC-conjugated antibodies from 1 hour to 30 days after injection. The black arrows indicate the intravitreal injection site. (*Top*) fluorescence microscopic image. (*Bottom*) Image developed by MATLAB. (A) FITC-conjugated whole IgG. (B) FITC-conjugated Fab fragments. (C) The representative images of the fluorescent gradient 3 days after IgG antibody intravitreal injection. Notice the fluorescent gradient from the center of vitreous to the peripheral vitreous and the ciliary body.

space, whereas the 250 nm (green F) nanoparticles did not. This finding indicates the movement of small molecules into the choroid through the uveal tissue, and they could reach the posterior retina including macula through this route. In the vitreous, the nondegradable nanoparticles seemed to be relatively stable, because the fluorescence intensity was uniform over time. Although the protein antibodies, such as IgG and Fab, are known to be smaller than the retinal layer nanopores and they penetrate the retina freely, nanoparticles accumulate on the inner retina, which is supported by previous animal experiments with gold nanoparticles.[25]

Intraocular Kinetics of Nanoparticles

The average optical density of fluorescence and the concentration of nanoparticles are summarized in Supplementary data: Supplementary Table S1 (25 nm micromer), Supplementary Table S2 (250 nm micromer), Supplementary Table S3 (50 nm Fluoresbrite), and Supplementary Table S4 (200 nm Fluoresbrite). Six time points (1 hour, 1 day, 7 days, 14 days, 21 days, and 30 days) were set for 25 nm and 250 nm nanoparticles, and five time points (1 hour, 1 day, 7 days, 14 days, and 30 days) were set for 50 nm and 200 nm nanoparticles, respectively. Figure 4 plots the graphs of the optical densities of the nanoparticles in the vitreous (Fig. 4A and 4B) and percentage ratio of the nanoparticles concentration in the vitreous after intravitreal injection (Fig. 4C), which shows a gradual decrease of nanoparticles according to their molecular sizes. From the data summarized in the supplementary tables, we derived the equations for the postinjection optical densities of various sized nanoparticles (Fig. 4A and 4B). Larger nanoparticles show relatively retained concentration level in the vitreous compared to the smaller nanoparticles. Overall, after the final 30 days postinjection period, the average percentage ratio of the nanoparticles is documented : 61.1% (25 nm), 69.1% (50 nm), 78.6% (200nm), and 85.3% (250 nm), which are statistically significant among each other (all $P < 0.001$, except 25 nm vs 50 nm [$P = .004$] and 200 nm vs 250 nm [$P = .005$]).

Table 2 summarizes the detailed PK parameters of different sizes of nanoparticles in the vitreous humor. The half-life of the nanoparticles are 50.94 days (25 nm red F), 48.78 days (50 nm Fluoresbrite), 66.65 days (200 nm Fluoresbrite), and 78.13 days (250 nm green F).

Discussion

In this study, we analyzed the intraocular distribution and kinetics of antibodies (whole IgG and Fab fragments) and nanoparticles. The results showed that the antibodies spread to the vitreous after 1 hour to 1 day after injection, started to clear after

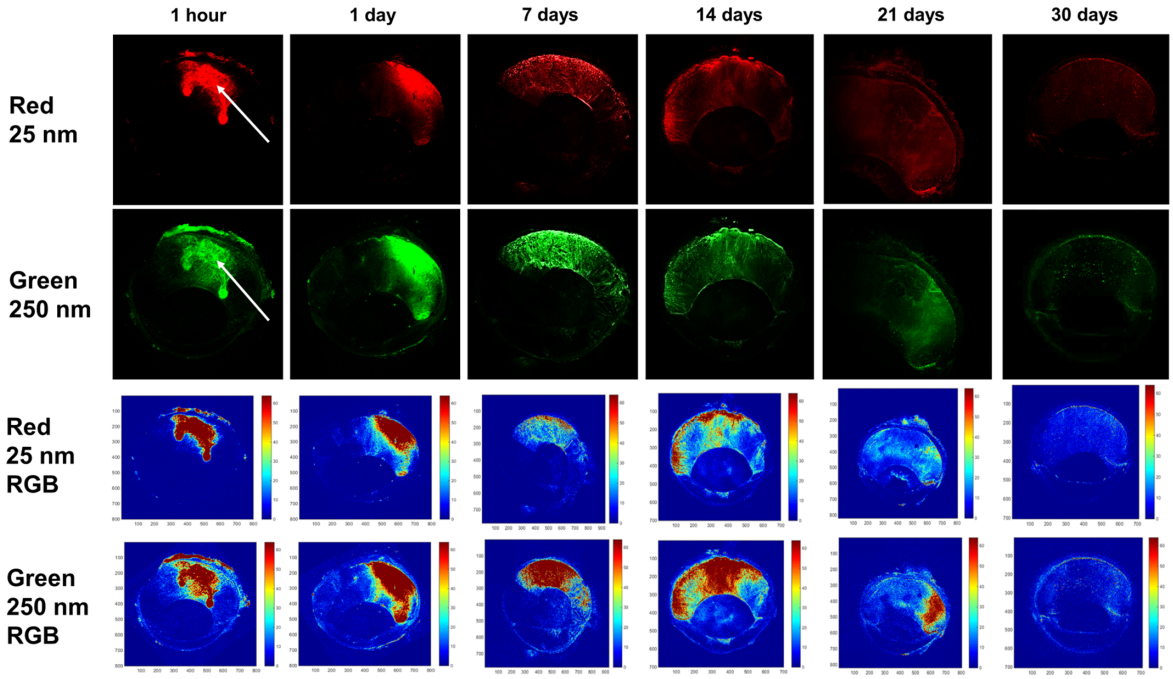

Figure 2. Serial images of the intraocular distribution of 25 nm (*red fluorescent*) and 250 nm (*green fluorescent*) nanoparticles observed at the different time points (1 hour, 1 day, 7 days, 14 days, 21 days, and 30 days) after the intravitreal injection. The RGB images were obtained by using a MATLAB image processing toolbox. After the intravitreal injection highlighted by *white arrows*, anteriorly and posteriorly spreading of nanoparticles were shown over time and maintained in the vitreous and accumulated in the retinal layer. Clearance and elimination after 21 days after injection were observed and in 30 days after injection, nanoparticles remained on the retinal inner surface while large portion of nanoparticles in the vitreous were removed.

3 days, and subsequently were not detectable at 25 days after the injection. On the contrary, nondegradable nanoparticles gradually decreased but maintained a relatively stable concentration in the vitreous humor, and elimination via the anterior chamber (aqueous humor) showed an initial increase and then a gradual decrease. Accumulation of nanoparticles in the retinal layer was observed by fluorescence microscopic images and small size 25 nm particles distributed to uveal tissue and suprachoroidal space, which resulted in the increased concentration in the posterior choroid and retina compartments.

In our previous studies,[17,18,20,21] the PK parameters of anti-VEGF agents (bevacizumab, ranibizumab, and aflibercept) were measured in the aqueous humor, vitreous, and retina in a New Zealand white rabbit model. With the animal experiment data, Ahn et al.[17,18] drew the standard curve for the bevacizumab and ranibizumab and calculated the intravitreal half-life, mean residence time, and clearance rate in the vitreous. From 1 to 3 days after injection, the concentrations showed a sudden decrease and then a gradual decrease until 30 days after injection when the antibodies could no longer be detected. This result coincides with our data in Figure 1, which illustrates the intraocular distribution of fluorescence-conjugated antibodies. The movement of Fab and IgG into the anterior chamber at day 1 could explain the initial sudden drop and the gradual disappearance of fluorescence inside the vitreous cavity from 3 to 10 days correlates with the gradual drug elimination after 3 days.

In this experiment, Figure 4 and the supplementary data show that the small size 25 nm and 50 nm particles seem to slowly decrease in the vitreous, whereas larger 200 nm and 250 nm particles are relatively stable. An explanation for this phenomenon may be that the elimination pathway system via the anterior chamber and ciliary body is easier for smaller size nanoparticles to pass through. Another explanation could be that the vitreous itself plays a role as a steric hindrance to molecular diffusion due to the rigid form of collagen and glycosaminoglycan.[26,27] Therefore, smaller nanoparticles migrate and diffuse in the vitreous and eliminate more rapidly than larger nanoparticles.

Our previous investigation suggests that Fc-free VEGF-Trap excretes more posteriorly than the VEGF-Trap molecule; thus, Fc-free antibodies are reported to have a higher preference to posterior distribution and clearance.[22] Therefore, the posterior

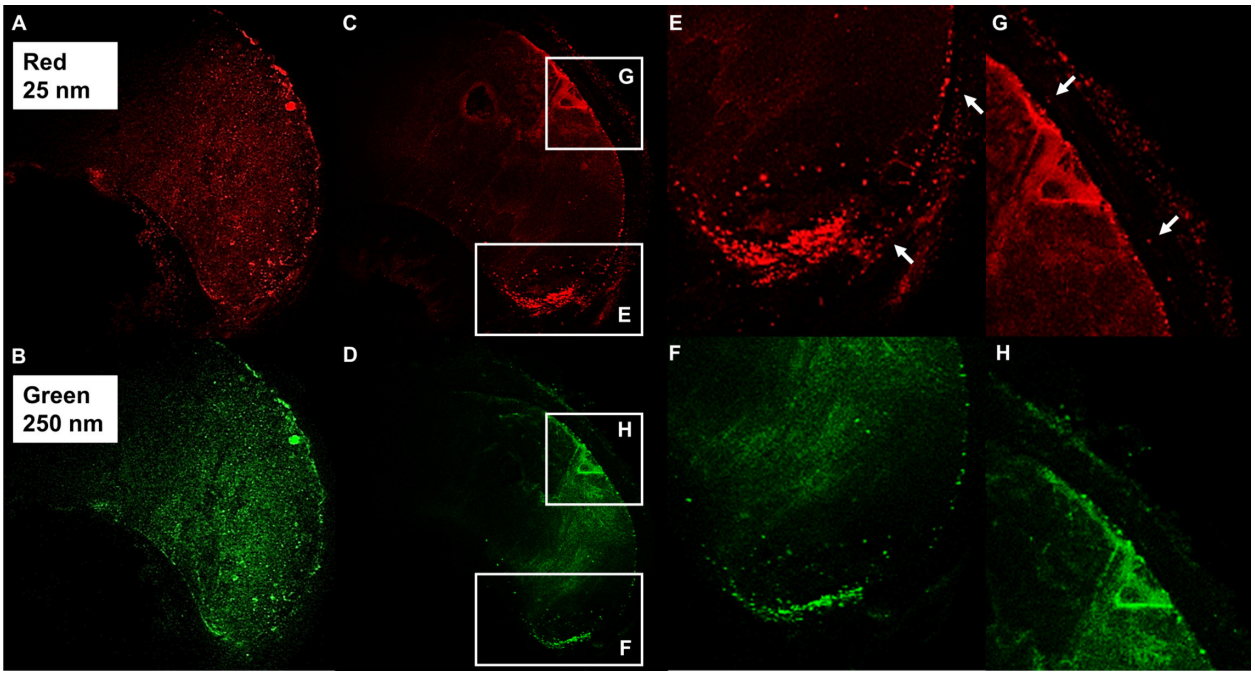

Figure 3. Confocal microscopic images of the intraocular and retinal distribution of intravitreally injected nanoparticles (25 nm, *red fluorescent*; 250 nm, *green fluorescent*). (A, B) Image taken at 14 days after injection. Nanoparticles spread to the posterior vitreous and accumulated in the retinal layers. (C, D) Images taken at 21 days after injection. The *red nanoparticles* were eliminated through the ciliary body and spread to the uveal tissue and suprachoroidal space. Conversely, green nanoparticles were not observed in the suprachoroidal space. (E–H) Magnified image of the retinal layer of red and green nanoparticles after 21 days after injection. The *white arrows* indicate the red nanoparticles in the choroid, retina, and suprachoroidal space.

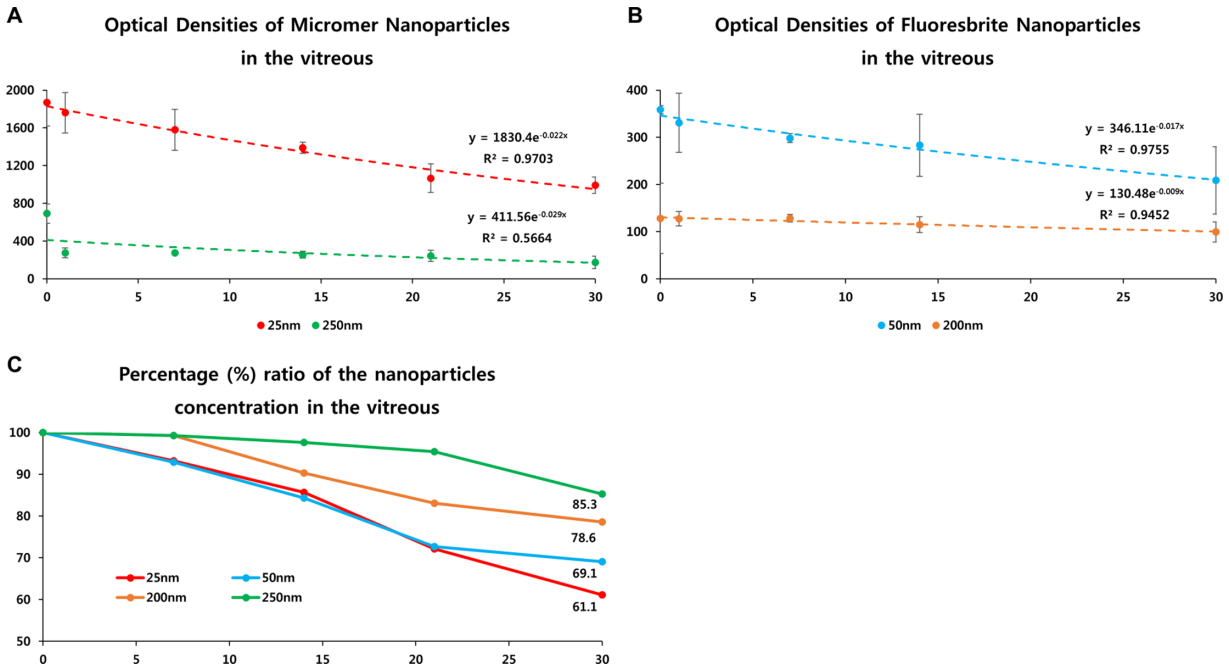

Figure 4. (A, B) Optical densities of the various-sized nanoparticles in the vitreous after the intravitreal injection. Exponential trendline curves are drawn and the equations and R^2 values are obtained. (C) The percentage ratio of the various-sized nanoparticle concentrations in the vitreous from 1 hour to 30 days of intravitreal injection. Smaller sizes of nanoparticles (25 nm and 50 nm) show a gradual decrease over time. On the contrary, larger sizes of nanoparticles (200 nm and 250 nm) show a slight decrease in the concentration after 1 day after injection. At 30 days after injection, the final percentage ratio is documented: 61.1% (25 nm), 69.1% (50 nm), 78.6% (200nm), and 85.3% (250 nm).

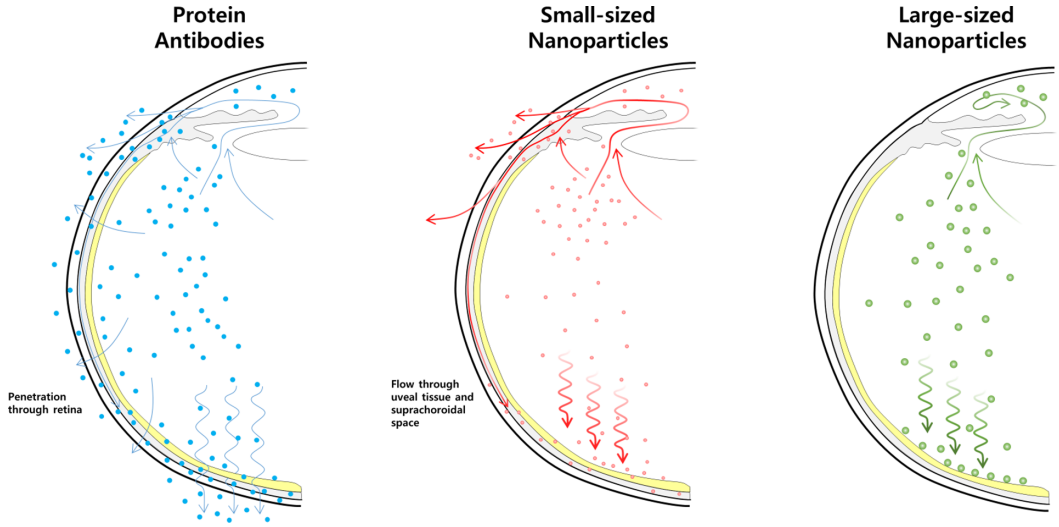

Figure 5. Intravitreal distribution of protein antibodies, small-sized nanoparticles, and large-sized nanoparticles. After the intravitreal injection, antibodies and nanoparticles spread to the anterior and posterior vitreous. Although protein antibodies such as IgG and Fab spread freely and penetrate the retinal layer, small-sized nanoparticles accumulate on the inner retina and were eliminated via two routes: (1) the anterior chamber and the (2) the ciliary body, uveal tissue and suprachoroidal space. Large-sized nanoparticles could not pass through the ciliary body and only accumulate on the inner retinal layer with no penetration.

aggregation of Fab fragments and fast elimination observed in Figure 1 could be explained. In addition, the fluorescence microscopic images of Figures 3A and 3B show that the nanoparticles attached to the retinal layer of the ILM regardless of particle size (25 nm red F and 250 nm green F). It is observed that the nanoparticles migrated to the posterior part of the ocular space and accumulated on the retinal surface, but did not penetrate the deeper retinal layers. This finding might be due to the structure of the ILM, which is composed of fine meshwork with many 10- to 20-nm nanopores.[28,29] On the contrary, antibodies have a hydrodynamic radius of 2.5 to 5.0 nm[11]; thus, ILM permeability could be measured and retinal/choroid elimination could happen. However, as shown in Figures 3C, 3E, and 3G, 25 nm red F nanoparticles pass across the ciliary body and move into the uveal tissue and suprachoroidal space after 21 days after injection, suggesting a somewhat activated posterior elimination pathway that could lead the small nanoparticles into the posterior choroid and retina. The schematic diagram figure of the intravitreal distribution of protein antibodies, small-sized nanoparticles, and large-sized nanoparticles is described in Figure 5.

In our experiment, we investigated the intraocular distribution and elimination of antibodies and nanoparticles of various sizes. Next, we need to study how to facilitate intraocular drug delivery and manage the sustained release of the drug. Ongoing studies are working on the improvement of intraocular drug delivery by the manipulation of antibodies and nanocarriers.[30–33] In terms of antibodies, a study by Joo et al.[22] proposed that the mutation of the Fc region could induce longer half-lives in vitreous and retina, contributing to the intraocular drug elimination. As for nanoparticles, surface charge and decoration significantly affect the intraocular distribution and drug delivery. The nanoparticles should be negatively charged (as in our studies) to avoid aggregation and immobilization since the vitreous matrix is anionic owing to collagen and glycosaminoglycan.[34] These polyanionic glycosaminoglycans such as hyaluronic acid and heparan sulfate are suggested as the key molecule for the charge-selective trapping ability of the vitreous humor, which is critical in intraocular diffusion.[35] Nanoparticle-coating techniques have been introduced to facilitate mobility. Recent studies by Martens et al. and Huang et al. suggest that hyaluronic acid–coated nanoparticles show increased efficacy of intraocular delivery with sustained and targeted uptake of nanoparticles by CD44 receptor ligands.[31,32,36] Moreover, the concept of retaining the therapeutic agents longer in the vitreous by hyaluronan-binding liposomes and microspheres has helped the vitrectomy surgery by prolonged visualization of the vitreous (US patent 2014/0186350 A1). Another experiment by Huang and Chau,[37] surface charge is crucial in regards to the intraocular distribution and the authors suggested the surface charge around +35 mV is optimal for the penetration of the retina. Therefore, further experiments regarding the specific modification of nanoparticle design with various molecular sizes

should be performed to observe the improvement of the delivery system.

In our study, there are some limitations to be considered. First, the study was performed as an animal model with New Zealand rabbit eyes. Thus, the intraocular distribution and kinetics might be different from those in human eyes. Even though the rabbit eye structure is similar to the human eye, the size of each compartment (aqueous humor, vitreous, and retina) and physical barriers (crystalline lens, ILM, and retinal pigment epithelium) are much smaller than the human eye. In addition, the vitreous flow pattern might be dissimilar, which affects the intraocular distribution of molecules. Therefore, the animal model results should be extrapolated to human eyes with caution. Second, at each time point, we humanely killed four rabbits and measured the average optical density and concentration in the right eyes. If we had increased the number of experimental subjects, more accurate data could have been drawn, especially in the nondetectable data in the Supplementary Tables S3 and S4 (50 nm and 200 nm nanoparticles). Third, the nanoparticle concentration level measured via fluorescence intensity might have been underestimated the actual number of nanoparticles and this could have caused inaccurate kinetic data. Last, we did not histologically evaluate the trabecular meshwork and did not measure serial intraocular pressure, which might affect the clearance and elimination phase. Further investigations are required to reveal the detailed data and mechanism of intraocular PKs of nanoparticles.

In conclusion, intraocular distribution and kinetics of antibodies and nanoparticles are different according to their molecular characteristics and size. Moreover, the concentration data of nanoparticles is evidence of anterior and posterior elimination pathways after intravitreal injection. The results of this study are essential to demonstrate that large numbers of nanoparticles are retained in the vitreous as compared to the antibodies due to the ILM barrier in the retina. Long-term retention of nanocarriers in the vitreous means prolonged intravitreal half-life and the sustained release of drugs in the intraocular space. Therefore, our results could provide foundational data in the development of newer intraocular drugs and carriers to treat retinal diseases.

Acknowledgments

Supported by a research grant from Seoul National University Bundang Hospital (06-2013-092 and 13-2015-012) and by the Bio & Medical Technology Development Program of the National Research Foundation (NRF) funded by the Korean government (MSIT) (No. 2018M3A9B5021319).

This work was completed in the Department of Ophthalmology, Seoul National University Bundang Hospital, 173-82 Gumi-ro, Bundang-gu, Seongnam-si, Gyeonggi-do, 13620, South Korea.

Disclosure: **H.M. Kim,** None; **S. Ha,** None; **H.K. Hong,** None; **Y. Hwang,** None; **P. Kim,** None; **E. Yang,** None; **J.Y. Chung,** None; **S. Park,** None; **Y.J. Park,** None; **K.H. Park,** None; **H. Kim,** None; **S.J. Woo**, Samsung Bioepis (C), Retimark (I), Novelty Nobility (S), Panolos Bioscience (C)

* HMK, SH, and HKH contributed equally to this work.

References

1. Rosenfeld PJ, Brown DM, Heier JS, et al. Ranibizumab for neovascular age-related macular degeneration. *N Engl J Med.* 2006;355:1419–1431.
2. Andreoli CM, Miller JW. Anti-vascular endothelial growth factor therapy for ocular neovascular disease. *Curr Opin Ophthalmol.* 2007;18:502–508.
3. Brown DM, Campochiaro PA, Bhisitkul RB, et al. Sustained benefits from ranibizumab for macular edema following branch retinal vein occlusion: 12-month outcomes of a phase III study. *Ophthalmology.* 2011;118:1594–1602.
4. Brown DM, Campochiaro PA, Singh RP, et al. Ranibizumab for macular edema following central retinal vein occlusion: six-month primary end point results of a phase III study. *Ophthalmology.* 2010;117:1124–1133, e1121.
5. Campochiaro PA, Brown DM, Awh CC, et al. Sustained benefits from ranibizumab for macular edema following central retinal vein occlusion: twelve-month outcomes of a phase III study. *Ophthalmology.* 2011;118:2041–2049.
6. Ferrara N, Damico L, Shams N, Lowman H, Kim R. Development of ranibizumab, an anti-vascular endothelial growth factor antigen binding fragment, as therapy for neovascular age-related macular degeneration. *Retina.* 2006;26:859–870.
7. Gaudreault J, Fei D, Beyer JC, et al. Pharmacokinetics and retinal distribution of ranibizumab, a humanized antibody fragment directed against VEGF-A, following intravitreal administration in rabbits. *Retina.* 2007;27:1260–1266.

8. Nomoto H, Shiraga F, Kuno N, et al. Pharmacokinetics of bevacizumab after topical, subconjunctival, and intravitreal administration in rabbits. *Invest Ophthalmol Vis Sci.* 2009;50:4807–4813.
9. Sinapis CI, Routsias JG, Sinapis AI, et al. Pharmacokinetics of intravitreal bevacizumab (Avastin(R)) in rabbits. *Clin Ophthalmol.* 2011;5:697–704.
10. Kim HM, Park KH, Chung JY, Woo SJ. A prediction model for the intraocular pharmacokinetics of intravitreally injected drugs based on molecular physicochemical properties. *Ophthalmic Res.* 2019:63:41–49.
11. Hutton-Smith LA, Gaffney EA, Byrne HM, Maini PK, Gadkar K, Mazer NA. Ocular pharmacokinetics of therapeutic antibodies given by intravitreal injection: estimation of retinal permeabilities using a 3-compartment semi-mechanistic model. *Mol Pharm.* 2017;14:2690–2696.
12. Bakri SJ, Snyder MR, Reid JM, Pulido JS, Ezzat MK, Singh RJ. Pharmacokinetics of intravitreal ranibizumab (Lucentis). *Ophthalmology.* 2007;114:2179–2182.
13. Bakri SJ, Snyder MR, Reid JM, Pulido JS, Singh RJ. Pharmacokinetics of intravitreal bevacizumab (Avastin). *Ophthalmology.* 2007;114:855–859.
14. Inokuchi Y, Hironaka K, Fujisawa T, et al. Physicochemical properties affecting retinal drug/coumarin-6 delivery from nanocarrier systems via eyedrop administration. *Invest Ophthalmol Vis Sci.* 2010;51:3162–3170.
15. Amrite AC, Edelhauser HF, Singh SR, Kompella UB. Effect of circulation on the disposition and ocular tissue distribution of 20 nm nanoparticles after periocular administration. *Mol Vis.* 2008;14:150–160.
16. Sakurai E, Ozeki H, Kunou N, Ogura Y. Effect of particle size of polymeric nanospheres on intravitreal kinetics. *Ophthalmic Res.* 2001;33:31–36.
17. Ahn J, Kim H, Woo SJ, et al. Pharmacokinetics of intravitreally injected bevacizumab in vitrectomized eyes. *J Ocul Pharmacol Ther.* 2013;29:612–618.
18. Ahn SJ, Ahn J, Park S, et al. Intraocular pharmacokinetics of ranibizumab in vitrectomized versus nonvitrectomized eyes. *Invest Ophthalmol Vis Sci.* 2014;55:567–573.
19. Niwa Y, Kakinoki M, Sawada T, Wang X, Ohji M. Ranibizumab and aflibercept: intraocular pharmacokinetics and their effects on aqueous VEGF level in vitrectomized and nonvitrectomized Macaque eyes. *Invest Ophthalmol Vis Sci.* 2015;56:6501–6505.
20. Park SJ, Oh J, Kim YK, et al. Intraocular pharmacokinetics of intravitreal vascular endothelial growth factor-Trap in a rabbit model. *Eye (Lond).* 2015;29:561–568.
21. Park SJ, Choi Y, Na YM, et al. Intraocular pharmacokinetics of intravitreal aflibercept (Eylea) in a rabbit model. *Invest Ophthalmol Vis Sci.* 2016;57:2612–2617.
22. Joo K, Park SJ, Choi Y, et al. Role of the Fc region in the vitreous half-life of anti-VEGF drugs. *Invest Ophthalmol Vis Sci.* 2017;58:4261–4267.
23. Hwang Y, Ahn J, Mun J, et al. In vivo analysis of THz wave irradiation induced acute inflammatory response in skin by laser-scanning confocal microscopy. *Opt Express.* 2014;22:11465–11475.
24. Choe K, Jang JY, Park I, et al. Intravital imaging of intestinal lacteals unveils lipid drainage through contractility. *J Clin Invest.* 2015;125:4042–4052.
25. Masse F, Ouellette M, Lamoureux G, Boisselier E. Gold nanoparticles in ophthalmology. *Med Res Rev.* 2019;39:302–327.
26. Park J, Bungay PM, Lutz RJ, et al. Evaluation of coupled convective-diffusive transport of drugs administered by intravitreal injection and controlled release implant. *J Control Release.* 2005;105:279–295.
27. Laude A, Tan LE, Wilson CG, et al. Intravitreal therapy for neovascular age-related macular degeneration and inter-individual variations in vitreous pharmacokinetics. *Prog Retin Eye Res.* 2010;29:466–475.
28. Nishihara H. [Studies on the ultrastructure of the inner limiting membrane of the retina. I. Surface replication study on the inner limiting membrane of the retina]. *Nippon Ganka Gakkai Zasshi.* 1989;93:429–438.
29. Nishihara H. [Studies on the ultrastructure of the inner limiting membrane of the retina–distribution of anionic sites in the inner limiting membrane of the retina]. *Nippon Ganka Gakkai Zasshi.* 1991;95:951–958.
30. Gan L, Wang J, Zhao Y, et al. Hyaluronan-modified core-shell liponanoparticles targeting CD44-positive retinal pigment epithelium cells via intravitreal injection. *Biomaterials.* 2013;34:5978–5987.
31. Huang D, Chen YS, Rupenthal ID. Hyaluronic acid coated albumin nanoparticles for targeted peptide delivery to the retina. *Mol Pharm.* 2017;14:533–545.
32. Martens TF, Remaut K, Deschout H, et al. Coating nanocarriers with hyaluronic acid facilitates intravitreal drug delivery for retinal gene therapy. *J Control Release.* 2015;202:83–92.

33. Martens TF, Vercauteren D, Forier K, et al. Measuring the intravitreal mobility of nanomedicines with single-particle tracking microscopy. *Nanomedicine (Lond)*. 2013;8:1955–1968.
34. Peeters L, Sanders NN, Braeckmans K, et al. Vitreous: a barrier to nonviral ocular gene therapy. *Invest Ophthalmol Vis Sci*. 2005;46:3553–3561.
35. Kasdorf BT, Arends F, Lieleg O. Diffusion regulation in the vitreous humor. *Biophys J*. 2015;109:2171–2181.
36. Koo H, Moon H, Han H, et al. The movement of self-assembled amphiphilic polymeric nanoparticles in the vitreous and retina after intravitreal injection. *Biomaterials*. 2012;33:3485–3493.
37. Huang X, Chau Y. Investigating impacts of surface charge on intraocular distribution of intravitreal lipid nanoparticles. *Exp Eye Res*. 2019;186:107711.